ACS NANO

www.acsnano.org

ARTICLE

Manufacturing mRNA-Loaded Lipid Nanoparticles with Precise Size and Morphology Control

Cedric Devos,[†] Aniket Udepurkar,[†] Peter Sagmeister,[†] Ariana S. Hodlewsky, Julie Chen, Andrew Hatas, Nicole Ostrovsky, Mushriq Al-Jazrawe, Joy I. Ren, Andy Y. Liu, Richard D. Braatz, and Allan S. Myerson*

Cite This: https://doi.org/10.1021/acsnano.5c09800

Read Online

ACCESS | Metrics & More | Article Recommendations | Supporting Information

ABSTRACT: **Lipid nanoparticles (LNPs) are the leading platform for delivering nucleic acid therapeutics, produced by rapidly mixing lipids in ethanol with nucleic acid cargo in an aqueous buffer. LNP production is often approached with a mixing-focused mindset that reduces the entire self-assembly process to a single step, obscuring the relationship between the process inputs and LNP properties. Here, we present a method for producing mRNA-loaded LNPs, with independent and predictive control over both the size and morphology and without compromising other quality attributes. By decoupling particle design from mixing and formulation changes, this method enables the rational engineering of LNPs with defined properties. The method leverages mixing under high fusogenicity conditions, achieved by modulating the solvent composition, followed by timed postinjection of an aqueous buffer to kinetically arrest LNPs at the desired properties. We demonstrate the method using benchmark LNP formulations in an impinging jet mixer, a state-of-the-art technology for LNP manufacturing. The resulting LNPs exhibit up to an 8-fold increase in *in vitro* transfection efficacy compared to those produced by the conventional method. In addition, the method facilitates quality control and supports predictive modeling and rational process translation.**

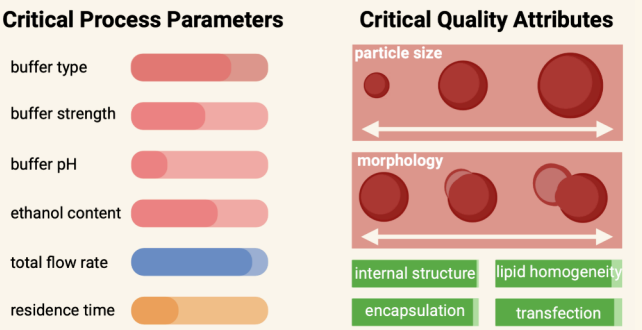

KEYWORDS: *lipid nanoparticle, mixing, size, morphology, formulation, nucleic acid, mRNA*

INTRODUCTION

Lipid nanoparticles (LNPs) have paved the way for a new generation of therapeutics based on nucleic acid delivery.[1−4] These therapeutics are promising for treating cancer,[5] infectious diseases,[6] and genetic diseases[4] by modulating gene expression and/or controlling protein synthesis. Once the target genetic sequence is known, nucleic acid-based therapeutics can be rapidly designed without altering the underlying production or delivery methods. Due to their large size, charge under physiological conditions, and fragility, nucleic acid-based therapeutics require the use of a delivery vehicle to cross biological barriers and prevent rapid degradation.[3,7] LNPs are the most clinically advanced and versatile delivery systems currently available for this purpose. Clinically approved LNP formulations consist of four lipid components—an ionizable lipid, a phospholipid, cholesterol, and a PEGylated lipid—at a specific molar ratio that encapsulate the nucleic acid.[1] The intense focus on expanding LNP functional capabilities through new formulations[8−12] has overlooked opportunities for significant improvements within established formulations.

LNP production currently follows a standardized continuous process: lipids solubilized in ethanol are rapidly mixed with an acidic aqueous buffer containing mRNA, followed by buffer exchange.[1] During the COVID-19 vaccine rollout, LNP manufacturing became a major bottleneck.[13] While early challenges stemmed from limited infrastructure and lipid supply, the enduring bottleneck lies in the intrinsic complexity of LNP self-assembly. Despite widespread use, LNP production lacks clear process−property relationships to guide the rational tuning of input parameters. The prevailing

Received: June 11, 2025
Revised: September 3, 2025
Accepted: September 4, 2025

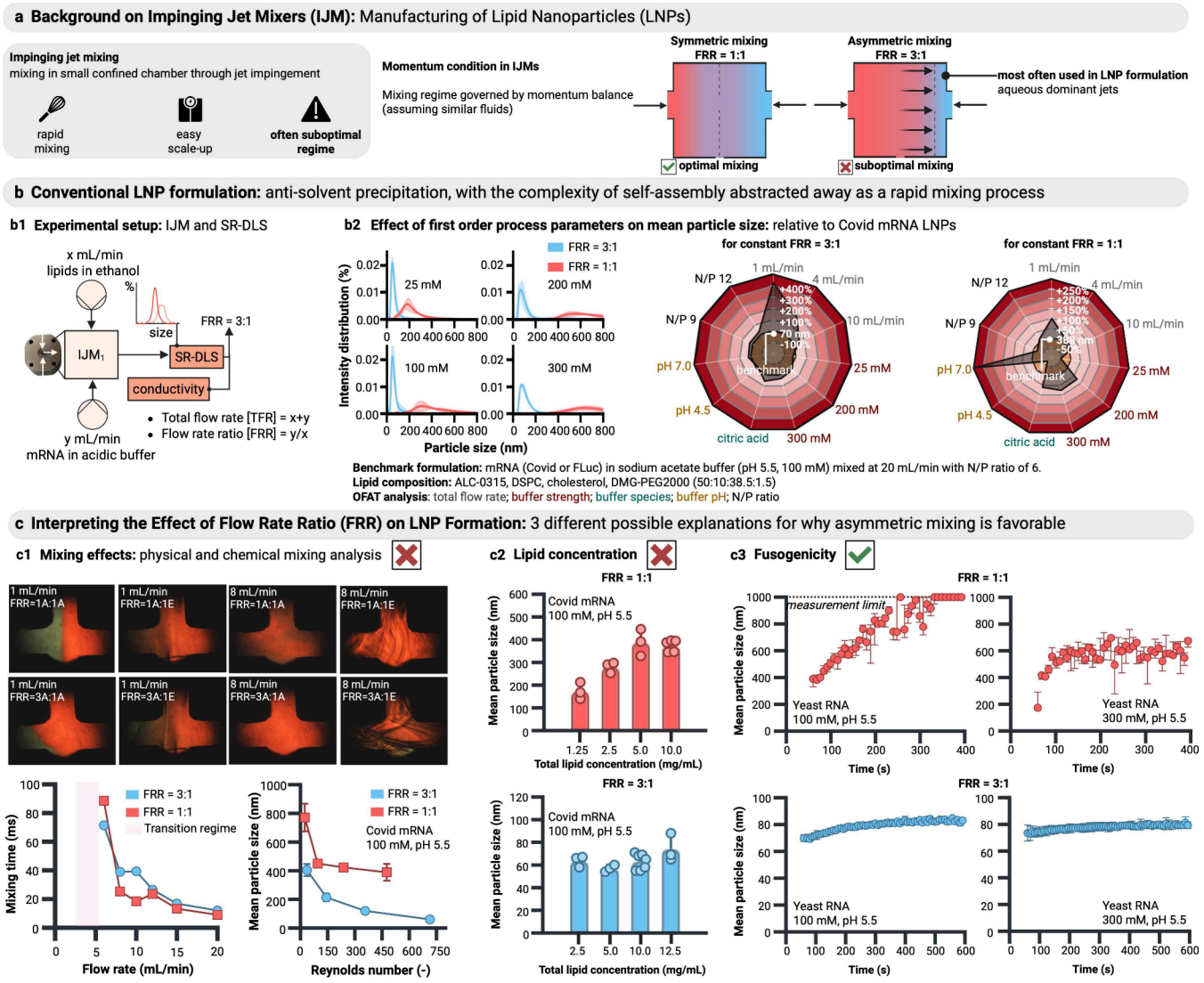

Figure 1. Understanding the role of the FRR in an IJM for LNP manufacturing. (a) Background on IJMs, which enable rapid, scalable mixing via jet impingement but are often operated in suboptimal regimes. (b) Effect of the FRR on LNP formation using a conventional continuous antisolvent precipitation approach. (b1) Schematic of the experimental setup consisting of an IJM coupled to a SR-DLS apparatus. (b2) Effect of the FRR on the particle size distribution at various buffer strengths for a benchmark formulation. The solid line represents the mean of triplicates, with the shaded region indicating the 95% confidence interval. OFAT sensitivity analysis of the mean LNP particle size for FRR = 3:1 and 1:1. The radar plot shows the percentage change in size relative to the benchmark condition. Each parameter (flow rate, buffer strength, buffer species, pH, and N/P ratio) is independently varied, while others are held constant. The results highlight the dominant influence of the total flow rate at FRR = 3:1 and the influence of buffer conditions at FRR = 1:1. (c) Three mechanistic interpretations evaluated to explain why the formulation at FRR = 3:1 improves LNP formation compared to the operation at FRR = 1:1 using the conventional production approach. (c1) Effect of mixing dynamics, assessed via physical dye tracer imaging (SI p 3), chemical tracer tests (mixing time vs flow rate, assessed with the Villermaux−Dushman protocol in the turbulent region, SI pp 4−7), and mean particle size as a function of the Reynolds number (SI p 2). The shaded area indicates the transition from laminar-to-turbulent mixing. (c2) Effect of increasing lipid concentration at FRR = 1:1 and 3:1 on the mean particle size. (c3) Role of the FRR in modulating self-assembly kinetics and fusion dynamics. The dashed line is for visual guidance of the measurement limit of the SR-DLS. The error bars represent the 95% confidence interval.

mixing-focused mindset treats LNP formation as a black-box outcome of rapid mixing. This approach reduces the multistage self-assembly into a single step, obscuring how input parameters (like flow rate, buffer strength, buffer species, etc.) shape key particle attributes, such as size, morphology, and structure.[1] In reality, LNP formation proceeds through sequential stages: initial assembly driven by amphiphilic lipid organization and electrostatic complexation with nucleic acids, followed by fusion, phase separation, and PEGylated lipid-mediated arrest, which collectively define the final size, morphology, and other quality attributes.

Size and morphology are two of the most recognized and widely reported quality attributes impacting the LNP efficacy. LNP size governs cellular uptake, circulation time, and tissue distribution,[7,14,15] while morphology, particularly the presence and fraction of blebbed LNPs, has been linked to the transfection efficacy.[16−18] Most published research on LNPs reports particles within the 60−120 nm range, but both smaller and larger sizes may offer application-specific benefits. The

https://doi.org/10.1021/acsnano.5c09800
ACS Nano XXXX, XXX, XXX−XXX

optimal size is determined by the therapeutic application, delivery route, and even species.[19] Although it is generally accepted that LNP self-assembly is known to be kinetically controlled, which implies that the rate and timing of intermediate steps control the outcome, this is seldom leveraged to guide or tune the formulation process. In conventional continuous LNP production, the mean particle size is largely governed by the mixing time,[1,20−22] yet the operational window is narrow: reduced mixing intensity leads to larger particles but also to poor encapsulation[14,21,22] and greater particle heterogeneity (for example, in terms of payload[23]). High mixing intensities reduce the particle size, but this effect plateaus quickly in the turbulent regime.[1,22] The buffer composition exerts a secondary influence,[17,24] although sometimes its influence may be too modest to have a meaningful impact.[25] As a result, the range of tunable particle sizes is often confined to a narrow, attainable region. The fraction of blebbed particles is usually modulated indirectly via buffer conditions[17] or flow structures,[21] which simultaneously also affects the particle size.[17] Regardless of which strategy is adopted to tune the LNP properties, the approach remains largely empirical and nonpredictive, with multiple quality attributes entangled to each other. Consequently, achieving the desired particle properties more often relies on high-throughput screening across different formulations,[18,26−28] until a potent formulation with suitable attributes is identified.

Here, we present a method that accounts for the multistep self-assembly process, enabling the deliberate design of LNPs with targeted size and morphology and maintaining or even enhancing other quality attributes. The approach is demonstrated using a custom impinging jet mixer (IJM) system coupled to a spatially resolved dynamic light scattering (SR-DLS) apparatus, allowing real-time, dilution-free measurement of particle size distributions immediately post formation and prior to buffer exchange. We show that this method enables rational, model-informed, and predictive process development, moving beyond the current inadequate approaches. Furthermore, it is robust, mixer-translatable, and versatile (in terms of lipid formulations and process conditions) and allows the design of LNPs with specific target properties, without the need to alter the formulation, to improve efficacy.

RESULTS AND DISCUSSION

Flow Rate Ratio Controls LNP Fusion. Conventional LNP production involves the rapid mixing of lipids in ethanol with nucleic acids in an acidic aqueous buffer, typically carried out at industrial scale using IJMs that enable high-throughput mixing via jet impingement in a small confined chamber.[29] Beyond maintaining a sufficiently high total flow rate to ensure turbulent, rapid mixing, a key operating parameter is the flow rate ratio (FRR), which in the case of LNPs is defined as the volumetric ratio of the aqueous (mRNA-buffer) to organic (ethanol-lipid) phase.[29] While IJMs are engineered for optimal performance at a FRR near 1:1,[29] where the momentum of both streams is balanced (Figure 1a), LNPs are consistently produced at FRRs of 3:1 to 10:1 with an excess aqueous phase.[1] As shown in Figure 1b, IJMs operated at FRR = 1:1 produce large, polydisperse particles, while operation at FRR = 3:1 consistently yields small, stable, uniform LNPs [Supporting Information (SI) pp 17, 18, and 26] with reasonable precision (SI p 27). Similar observations have been documented previously.[22,30] LNPs formed at FRR = 1:1 also exhibit poor lipid homogeneity (SI pp 17 and 18) and suboptimal internal structure (lamellar structure, SI p 28) for transfection compared to those generated at FRR = 3:1 (inverse hexagonal structure, SI p 28). One-factor-at-a-time analysis (OFAT; Figure 1b2, visualized as radar plots) shows that, at FRR = 3:1, the LNP size is primarily governed by the total flow rate (i.e., mixing), whereas at FRR = 1:1, it is dictated by the solution composition (e.g., buffer strength/species). A study of the effect of different inputs on the particle size distribution for the conventional LNP production method is provided in SI pp 16−26, including the effect of the total flow rate (SI p 17), FRR (SI p 18), N/P ratio (SI p 19), ionizable lipid (SI p 20), buffer molarity (SI p 21), pH (SI p 22), buffer species (SI p 23), total lipid concentration (SI p 24), and cargo (SI p 25).

To investigate why the operation at FRR = 3:1 produces LNPs with smaller sizes and narrower distributions than FRR = 1:1, we evaluated three hypotheses (Figure 1c): (i) improved mixing occurs at FRR = 3:1; (ii) higher lipid concentration leads to a higher driving force for LNP self-assembly;[30] (iii) differences in LNP fusion dynamics. Chemical and physical tracer studies confirm that mixing at FRR = 1:1 is marginally faster than that at FRR = 3:1 (Figure 1c and SI pp 3−7), consistent with the IJM literature[29] and prior work in the LNP field,[22] eliminating mixing efficiency as a primary driver to explain the difference between LNPs produced at FRR = 3:1 and 1:1. Lipid concentration effects were modest and insufficient to explain the observed size differences (Figure 1c and SI p 24). In contrast, time-resolved size measurements revealed that LNPs at FRR = 1:1 continue to increase in size, while those at FRR = 3:1 remain roughly the same size (Figure 1c). This size increase can be attributed to LNP-LNP fusion: At FRR = 1:1, the higher ethanol content increases lipid membrane fluidity by disrupting lipid packing,[31−33] thereby lowering the energy barrier for fusion. Membrane fusion is known to influence both structural and morphologhical aspects of lipid-based particles.[34−37]

LNP fusion has gained significant attention in recent years.[17,36−38] The results in Figure 1c suggest that the fusion dynamics can be strategically leveraged during formulation at FRR = 1:1. Higher ethanol content at FRR = 1:1 prolongs the fusion-prone window, during which nascent LNPs remain dynamic and capable of further growth via fusion before being kinetically arrested. While FRR is known to influence the particle size[1,19,28] and extended hold times (in the hour-scale, which is unsuitable for manufacturing purposes) promote fusion-driven growth,[19] these effects have not been exploited in a controlled manner. In conventional formulation at FRR = 3:1, fusion does not appear rapidly enough to be effectively harnessed, despite attempts to control it through PEG postaddition,[39,40] or buffer species and molarity.[17] Other studies[35] may have overlooked the potential for harnessing the fusion dynamics due to limitations in analytical resolution immediately postformulation.

Size-Controlled LNP Production. LNP−LNP fusion can be rapidly halted by injecting additional aqueous buffer, which sharply reduces the ethanol content and kinetically arrests the particle dynamics and interactions. By precise control of the time between the initial formulation and this postinjection step (defined by a residence time, here varied between 5 and 440 ms), the final particle size can be predictably and reproducibly tuned, beyond what has been demonstrated previously. To fully exploit this tunability, the initial formulation is ideally performed at FRR = 1:1, where solution conditions (e.g., buffer strength and composition) have a stronger influence on the

https://doi.org/10.1021/acsnano.5c09800
ACS Nano XXXX, XXX, XXX−XXX

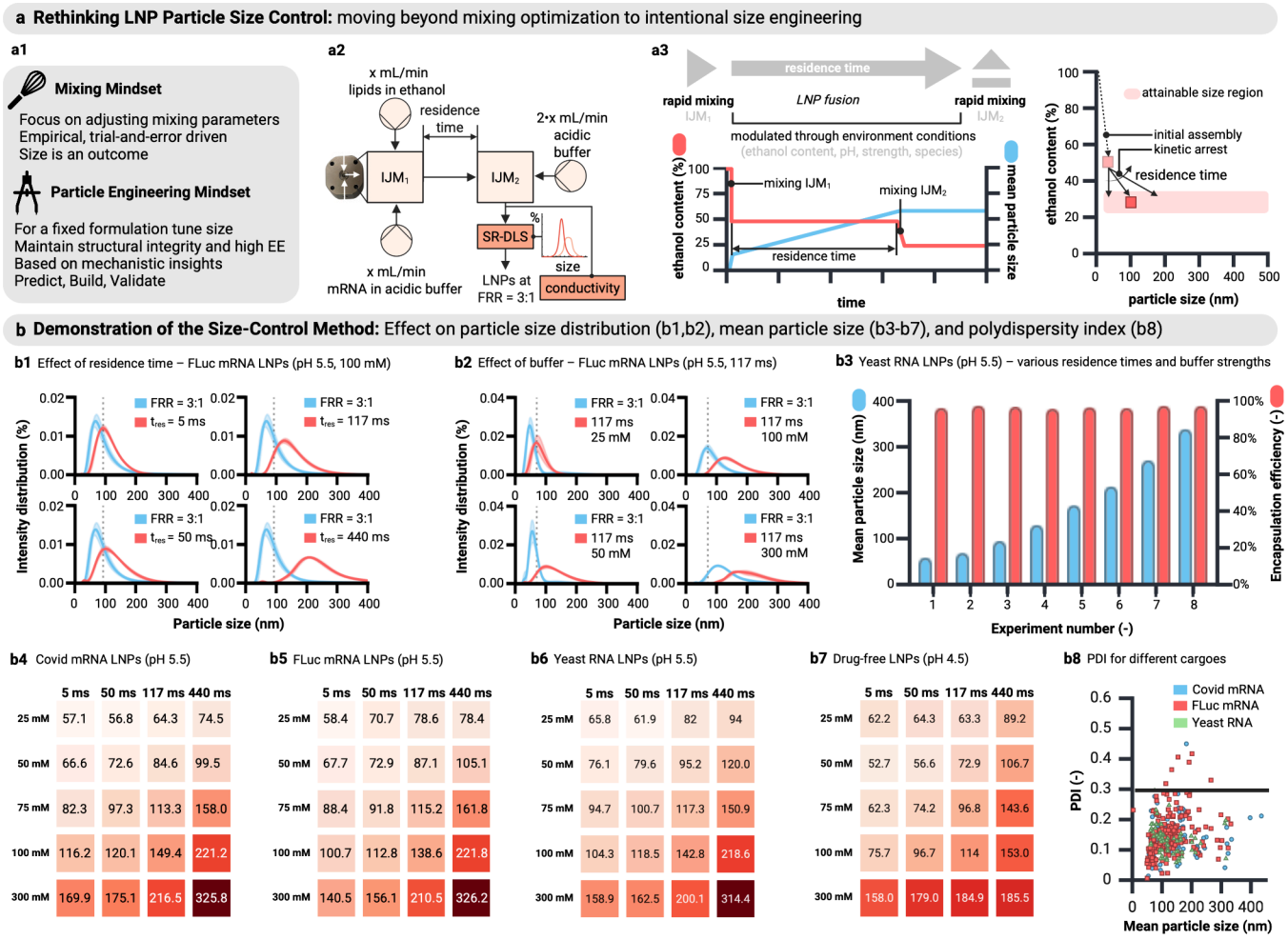

Figure 2. Introducing the size-control method for engineering LNPs with defined particle sizes. (a) Concept underlying the size-control method. (a1) Conceptual shift from a conventional "mixing mindset" to a particle engineering approach focused on intentional size control. (a2) Schematic of the experimental setup implementing the size-control method. (a3) Mechanistic concept: using symmetric mixing (FRR = 1:1) to exploit rapid fusogenicity and solution composition sensitivity, followed by kinetically arresting fusion at a defined residence time to reduce the ethanol content and lock in the target particle size. (b) Experimental demonstration of the method for a benchmark formulation. Effect of the (b1) residence time and (b2) buffer strength on the particle size distribution with the size-control method. The dashed line is for visual guidance. The solid line represents the mean of triplicates, with the shaded region indicating the 95% confidence interval. (b3) Encapsulation efficiencies for LNPs with a different mean size produced with the size-control method by varying the residence time (5−440 ms) and buffer strength (25−300 mM). (b4−b7) Mean particle size across triplicates for various residence times (columns) and buffer strengths (rows), applied to a benchmark LNP formulation with different cargos and formulated at pH 5.5 or 4.5. Color intensity scales with the particle size. (b8) PDI for LNPs produced by using the size-control method. The solid line for PDI at 0.3 represents the regulatory limit.

particle size (Figure 1b). In contrast, at FRR = 3:1, the size is predominantly governed by mixing (Figure 1b) and LNP−LNP fusion is limited, offering less opportunity for tunability through the solution composition. The size-control method is demonstrated conceptually in Figure 2a and experimentally for a benchmark formulation in Figure 2b. Although not strictly required, higher quench volumes are also effective (SI p 39), and two volumes of aqueous buffer are injected in the experimental demonstration to enable a direct comparison with conventional LNP production at FRR = 3:1. Specifically, Figure 2b shows how it is the combination of the solution composition and residence time that controls the particle size distribution and mean particle size.

Use of the size-control method increases the attainable mean particle size region considerably compared with conventional production at FRR = 3:1. Figure 2b shows the mean size range (50−400 nm) of the LNPs produced using the size-control method for different cargoes by manipulating the residence time and buffer conditions, while meeting the conventional standard of low polydispersity index (PDI; <0.3) and high encapsulation efficiency (EE; >80%). The particle size distributions obtained by using the size-control method have a PDI below the typical limit of 0.3 (Figure 2b8) and are not statistically significantly different from the LNPs produced with conventional methods. Although intrinsically the method is particularly suitable for the formation of larger LNPs—often difficult to produce with conventional approaches—by leveraging fusion-driven growth prior to kinetic arrest, under specific conditions, it also yields smaller particles with narrower PDI compared to conventional methods (Figure S19), assuming identical buffer species, strength, and pH; this includes LNPs of around 50 nm (Figure S19), with further reductions potentially achievable. The ability to generate smaller particles is primarily due to improved mixing in the initial stage at FRR = 1:1 compared with conventional FRR = 3:1 conditions.

https://doi.org/10.1021/acsnano.5c09800
ACS Nano XXXX, XXX, XXX−XXX

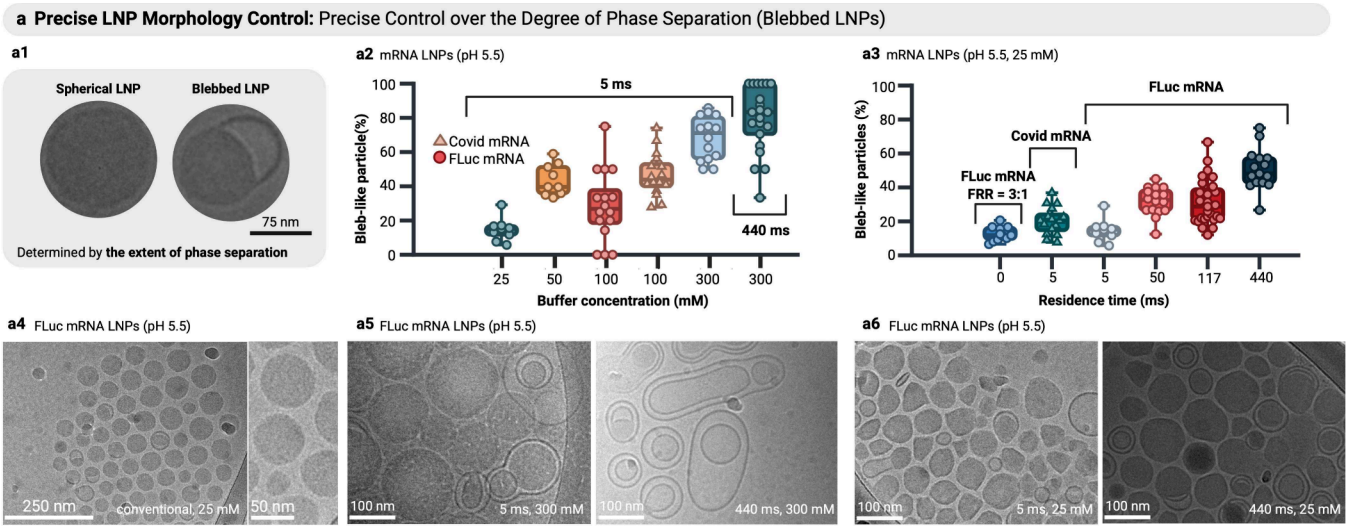

Figure 3. Introducing the morphology-control method for engineering LNPs with defined degrees of phase separation (blebbed LNPs). (a) Experimental demonstration using selected benchmark formulations. (a1) Comparison of spherical vs blebbed LNPs, based on the extent of phase separation and the presence of an electron-lucent compartment (as observed in cryoTEM images). (a2 and a3) Effect of the buffer concentration and residence time on the bleb fraction. Bars represent the mean across replicates, with error bars indicating the 95% confidence intervals. Different cargoes (Covid mRNA vs FLuc mRNA) are compared to highlight the robustness of the method. (a4−a6) CryoTEM images illustrating morphological differences across LNPs with different degrees of phase separation and bleb fractions.

Conversely, the method also enables facile production of larger LNPs (>200 nm), a size range that has been relatively underexplored, likely due to the difficulty of generating such particles while maintaining payload encapsulation using conventional approaches. Despite this, such particles hold therapeutic potential because they are more efficiently taken up by immune cells (like monocytes, macrophages, and dendritic cells), employing phagocytosis and macropinocytosis.[41] Okuda et al.[24] demonstrated that modulating buffer conditions can generate mRNA-loaded LNPs larger than 200 nm although at the cost of reduced EE—unlike the method presented here—and that these larger particles led to higher transgene expression in mouse splenic dendritic cells. Similarly, Kranz et al.[42] showed that lipid-based nanoparticles in the 200−400 nm range performed well for intravenous cancer immunotherapy, achieving efficient delivery to splenic dendritic cells. Recently, also Hu et al.[43] found that particles with an average size of 400 nm are optimal for efficiently transfecting monocytes following intravenous administration.

The proposed method moves beyond the conventional focus on mixing alone and opens the door to engineer the LNP size through controlled postformulation. While rapid mixing remains important in the initial stage to initiate self-assembly and sufficiently fast mixing is still required for the kinetic quench, this method reframes LNP self-assembly as a two-stage process. Notably, because both stages are operated at FRR = 1:1, optimal jet impingement conditions are met, making rapid mixing easier to achieve. A study on the effect of different inputs on the particle size distribution for the size-control LNP production method is provided in SI pp 29−39, including the effect of the residence time and buffer molarity (SI pp 30−34), pH (SI p 35), buffer species (SI p 36), total flow rate (SI p 37), N/P ratio (SI p 38), and final FRR (SI p 39). For brevity, LNPs produced using FRR = 1:1, followed by a timed residence period, and postinjection of two volumes of buffer are referred to as size/morphology-controlled LNPs, while those produced using FRR = 3:1 are referred to as conventional LNPs.

Morphology-Controlled LNP Production. Morphology is determined by analyzing cryoTEM images, which is, despite its limitations, the most direct and definitive technique to characterize LNP morphology,[1] shown in Figure 3a. Prior studies have shown that, following the initial mixing, LNPs can undergo pH-triggered fusion, which is eventually arrested by PEGylated lipid saturation, suggesting that the final morphology emerges from kinetically controlled fusion processes.[38] In the presented approach, fusion is deliberately accelerated by modulating the ethanol content (via operation at FRR = 1:1) and buffer conditions, without the need for a pH-trigger, and then arrested through a timed kinetic quench. The buffer quench kinetically arrests lipid organization, preventing equilibration and eliminating the need for changes in the formulation to incorporate lipids that artificially promote lipid−lipid demixing. As a result, the size-control method also modulates the morphology, specifically, the extent of phase separation and bleb formation, orthogonally to the particle size (see further). This is experimentally demonstrated for a benchmark formulation in Figure 3, with a level of control not previously reported and over a considerably larger range than is achievable with established approaches. For example, while our method tunes the bleb fraction from 12% to 80% for a benchmark formulation (Figure 3), changing the buffer from 25 to 300 mM in prior work (for the same benchmark formulation) only achieved a narrower range of 40−55%.[17]

Additional cryoTEM images of LNPs produced via the morphology-control method, for different cargoes, buffer strengths, and residence times, are provided in SI pp 43−46.

Orthogonal Control of the LNP Size and Morphology. As the size/morphology-control method introduces the residence time as an independent input parameter, it enables decoupling of the size and morphology. To demonstrate such orthogonal and predictive control over the LNP size and morphology, three case studies were performed: two targeting specific mean sizes (e.g., 70 and 115 nm) with variable bleb fractions and one targeting a specific bleb fraction (30%) with

https://doi.org/10.1021/acsnano.5c09800
ACS Nano XXXX, XXX, XXX−XXX

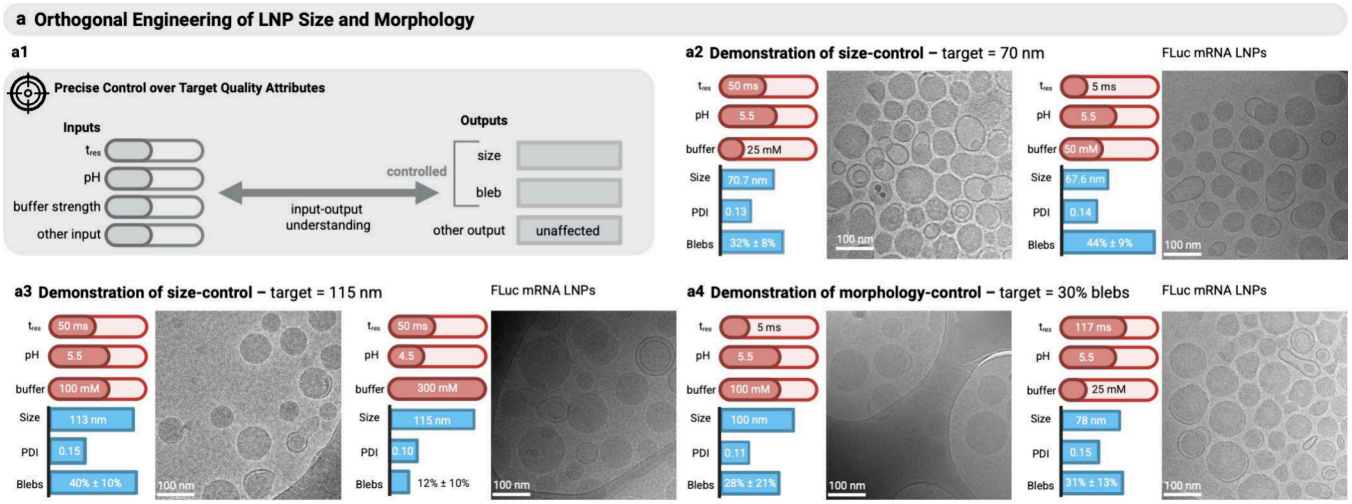

Figure 4. Experimental demonstration of the size/morphology-control method for engineering LNPs. (a1) Conceptual overview illustrating orthogonal control of the particle size and bleb fraction through independent tuning of the input parameters. (a2–a4) Demonstration of the orthogonal size and morphology control for different target sizes (a2 and a3) and target bleb fractions (a4) for the benchmark formulation. The inputs (rounded red bars) correspond to process parameters varied here (residence time, pH, and buffer strength), while the outputs (blue rectangles) report measured particle characteristics (size, PDI, and bleb fraction). Each experimental condition is accompanied by a cryoTEM image.

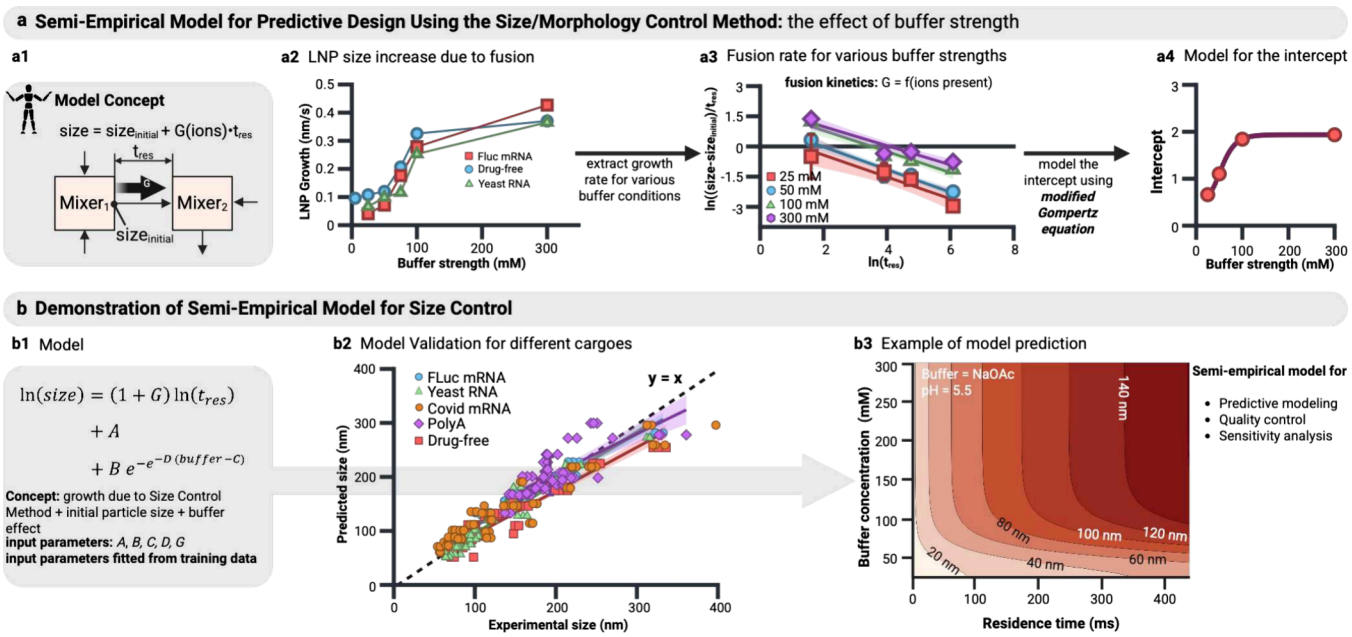

Figure 5. Predictive data-driven model for the size-control LNP formulation method. (a) Development of a semiempirical model. (a1) Conceptual framework. The LNP size evolution is modeled as the sum of two terms: initial self-assembly in the first mixer and subsequent growth during residence time, both dependent on the buffer strength. (a2) Experimental data showing the LNP growth rate prior to kinetic arrest as a function of the buffer strength. (a3) log–log plot of growth rate versus residence time across different buffer strengths. (a4) Estimation of the initial size (intercept) using a modified Gompertz equation, parametrized by the buffer strength. (b) Application of the semiempirical model for predictive control. (b1) Fitting model parameters to the experimental data. (b2) Parity plot comparing predicted versus experimentally measured particle sizes across multiple nucleic acid cargos, indicating high agreement between the model and experiment. (b3) Example of a sensitivity analysis predicting the final mean particle sizes across the residence time and buffer conditions. Contours indicate predicted mean particle sizes (in nanometers), with lighter regions corresponding to smaller sizes.

variable particle sizes. Results for a benchmark formulation are shown in Figure 4.

Orthogonal control, as shown in Figure 4, is enabled by independently tuning multiple parameters, such as the buffer strength and residence time, to access distinct morphologies at a fixed particle size. In contrast, single-parameter approaches (e.g., buffer strength alone) simultaneously affect both the size and morphology, often within a limited range dependent on the ionizable lipid. For the same LNP formulation, the reported 15% increase in the bleb fraction required simultaneously increasing the particle size from 46 to 130 nm and reducing EE from 84% to 72% (see further).[17] As shown in Figure 4a2, a bleb fraction increase of nearly 15%

https://doi.org/10.1021/acsnano.5c09800
ACS Nano XXXX, XXX, XXX–XXX

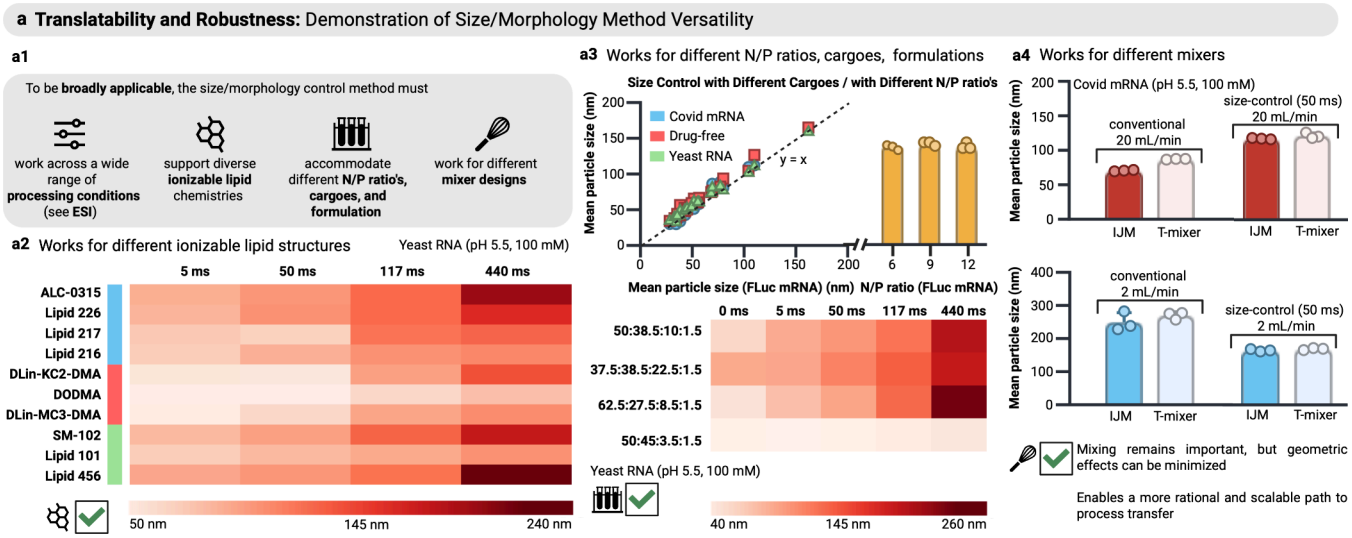

Figure 6. Translatability and robustness of the size/morphology-control method. (a1) Schematic illustration of translatability and robustness in the context of LNP manufacturing. Experimental demonstration that the method enables consistent control of the size and morphology across (a2) different ionizable lipid structures (each row represents an LNP formulation with a distinct ionizable lipid; see the SI), (a3) varied N/P ratios, cargos, and formulations, and (a4) multiple mixer designs using selected benchmark formulations. In the heatmaps in parts a2 and a3, the color intensity scales with the mean particle size. In part a2, ionizable lipids are grouped by structural class: the ALC-0315 class (blue), the DLin-KC2-DMA class (red), and the SM-102 class (green). In part a3, each row represents a different molar ratio of ionizable lipid/cholesterol/phospholipid/PEG-lipid. The dashed line in part a3 is for visual guidance.

does not necessarily require an increase in the particle size using the size/morphology-control method.

Predictive Data-Driven Model. The size/morphology-control method conceptualizes LNP formation as a two-step process: an initial self-assembly phase, which remains poorly understood due to the lack of techniques with sufficient temporal and spatial resolution, followed by a fusion-driven size-increase phase that can be modulated via solution conditions and arrested at a defined time. A key advantage of this approach is that the second stage can be readily modeled by using a data-driven regression framework and the initial self-assembly size can be extrapolated from the experimental data. While not fully mechanistic, this strategy enables predictive control well beyond what is offered by current LNP formation models.[44]

Such a data-driven model was developed for a benchmark formulation, as shown in Figure 5a, using multiple linear regression. The model captures the influence of the buffer strength and residence time (t_{res}) and is further generalized by incorporating the pH and conductivity [G(ions)] to enable prediction beyond the initially tested conditions. The model requires the fitting of five model parameters. The model is validated in Figure 5b and used to conduct a sensitivity analysis. It demonstrates improved predictive accuracy relative to the existing models (Figure 5b2 parity plot). Additional information regarding the predictive model is provided in SI pp 48−52. Experimentally, the size/morphology-control method offers the added advantage of simplified process monitoring because key input parameters, the buffer strength and pH, can be tracked using a low-cost conductivity probe and directly incorporated into the predictive model.

Robustness and Versatility of the Size/Morphology-Control Method. The size/morphology-control method is broadly applicable because it demonstrates robustness across different formulations (beyond the benchmark formulation used in the rest of this work), processing conditions, and mixer designs. Figure 6 illustrates the versatility of the method. It demonstrates that the method works for precise control of the particle size across a diverse set of ionizable lipids (Figure 6a2), N/P ratios, cargo types, and formulation composition ratios (Figure 6a3).

Notably, different ionizable lipid structures exhibit distinct fusion rates: several current-generation lipids (e.g., DLin-MC3-DMA, ALC-0315, and SM-102), optimized for endosomal escape via membrane fusion, have rapid LNP−LNP fusion during formulation. Additionally, yeast RNA and poly(A) effectively serve as low-cost mRNA surrogates in the size-control method, with quality attributes obtained with the surrogates matching well with purified mRNA. Drug-free LNPs exhibit size-control trends similar to those of loaded particles but are significantly smaller at pH 7.0 and larger at pH 4.5 due to pK_a-dependent charge effects, with size convergence at pH 5.5 further demonstrating that the method generalizes across cargo types.

Importantly, the size/morphology method performs consistently across mixer geometries (Figure 6a4; IJM versus T-mixer). This is a result of a reduced sensitivity to the mixing time (although rapid mixing is still required in the first mixer) and an increased sensitivity to the solution composition due to the operation at FRR = 1:1 instead of FRR = 3:1, as shown in Figure 1b. This is a major advantage for any manufacturing method because it allows implementation with other mixer geometries, making it easily integrable into existing LNP production platforms for companies that have already locked-into specific technology. For the same reason, the mean particle size for the operation at low mixing speeds (2 mL/min) is far less affected than that for the conventional formulation. The size/morphology-control method thus allows for a more rational process translation between different mixers and facilitates easier scale-up.

Implications of Size/Morphology Control. While size and morphology are key, other quality attributes, such as EE,

https://doi.org/10.1021/acsnano.5c09800
ACS Nano XXXX, XXX, XXX−XXX

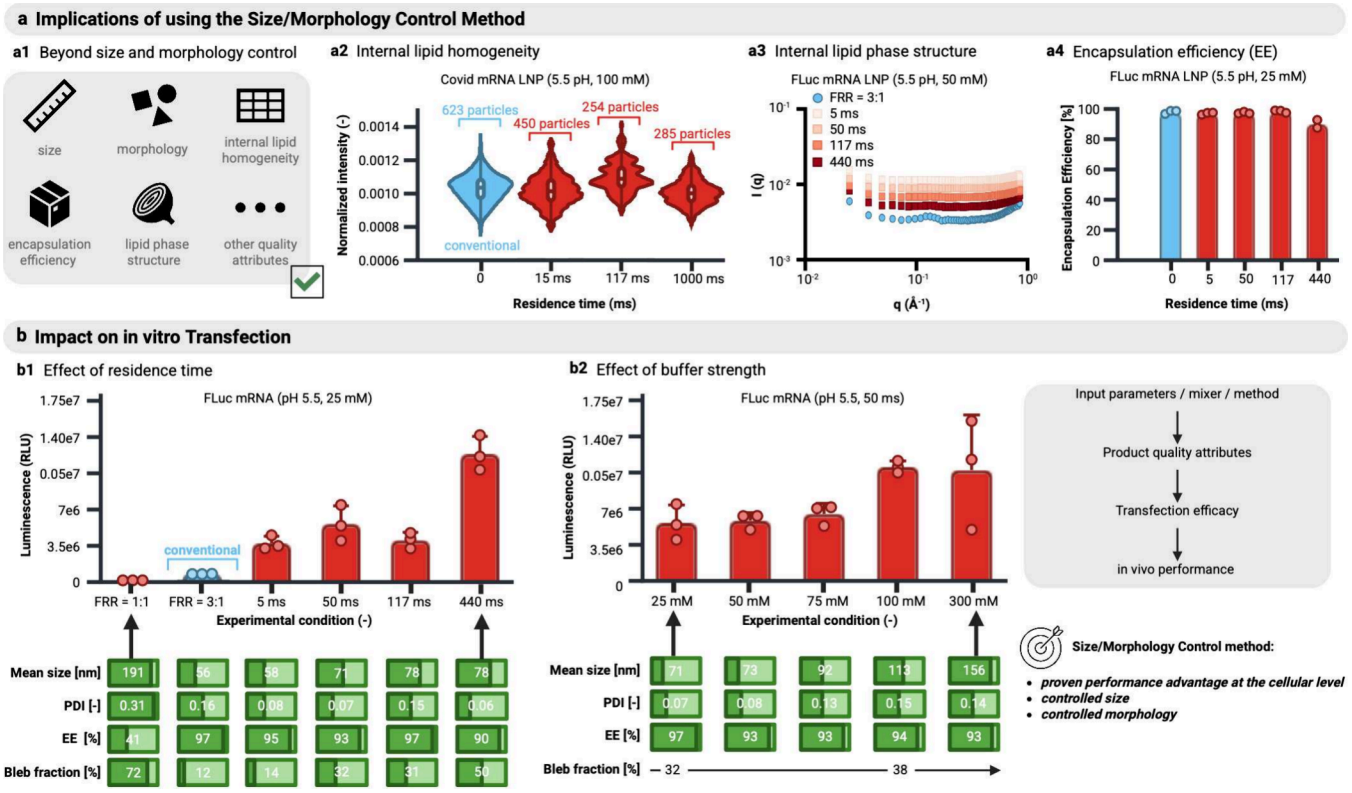

Figure 7. Implications of size-controlled LNP manufacturing on quality attributes and in vitro transfection. (a) Overview of how the size/morphology-control method influences quality attributes beyond the particle size and morphology for a benchmark formulation. (a1) Identification of relevant quality indicators. Demonstration that the method preserves (a2) internal lipid homogeneity measured using SPARTA, (a3) internal lipid phase structure measured using SAXS, and (a4) EE measured using the RiboGreen Assay, exceeding the best outcomes from conventional LNP formulations. Violin plots in part a2 show the distribution of normalized ionizable lipid Raman intensity across individual LNPs (the number of LNPs measured is shown), reflecting the relative lipid content and enabling a comparison of compositional homogeneity on an intraparticle level within an LNP solution. (b) Evaluation of in vitro transfection using LNPs produced via the size- and morphology-control method for selected benchmark formulations. (b1 and b2) Transfection results showing that the method enables engineering of LNPs with increased transfection performance through improvements in specific key quality attributes, while maintaining others (such as EE) constant.

internal structure, and lipid homogeneity, also play a role in determining LNP efficacy. Other size- or morphology-control strategies often lack specificity; for example, reducing the total flow rate to increase the particle size compromises the EE. In one case using a ring micromixer, LNPs produced at 0.4 mL/min exhibited a mean size of 183 nm with only 60% EE (thus falling below typical threshold values), compared to 97 nm and 82% EE at 8 mL/min.[22] This intrinsic coupling of quality attributes complicates meaningful comparisons between formulations, highlighting a key advantage of the size/morphology-control method.

As shown in Figure 7, LNPs produced using the size/morphology-control method exhibit quality attributes comparable to those generated via the conventional method at FRR = 3:1. Both approaches result in similar final ethanol contents, ensuring equivalent stability profiles. Figure 7a2 shows that lipid homogeneity, assessed by single particle Raman trapping analysis (SPARTA), is maintained, indicating a consistent ionizable lipid distribution across particles. Small-angle X-ray scattering (SAXS) data (Figure 7a3) confirm that all LNPs adopt an inverse hexagonal internal phase through equilibration, regardless of the residence time (SI p 40. This suggests that the internal structure—unlike the mean particle size, morphology, or EE—may be governed by thermodynamic rather than kinetic control. Due to improved mixing in the size/morphology-control process (Figure 1c1), the EE remains high, with near-complete cargo loading. Researchers at AstraZeneca increased the mean LNP size from 73 to 147 nm, but at the cost of reducing the EE from 96% to 74%.[14] To our knowledge, no existing method, apart from the size/morphology-control approach presented here, allows size tuning while maintaining other quality attributes such as the EE.

To assess whether these preserved quality attributes translate into functional performance, we evaluated the in vitro transfection efficiency of LNPs produced using the size- and morphology-control method (Figure 7b and SI p 47). LNPs engineered using the size- and morphology-control method consistently achieved higher in vitro transfection across multiple conditions compared with those produced via the conventional approach (Figure 7b), demonstrating a clear cellular-level advantage. In vitro transfection levels can correlate with in vivo protein expression, making them a critical indicator for the final LNP efficacy. The increased cellular-level performance observed with our method thus provides a strong foundation for in vivo success.

While limited in vitro data preclude definitive conclusions across cell lines and different LNP formulations, our results suggest a positive correlation between the bleb fraction and transfection performance. An exception is observed for LNPs

https://doi.org/10.1021/acsnano.5c09800
ACS Nano XXXX, XXX, XXX−XXX

produced at FRR = 1:1 without the size/morphology-control method, which show markedly reduced efficacy, which can be attributed to poor EE.

OUTLOOK

This paper introduces an LNP design and engineering approach, as often advocated for in other pharmaceutical particle processes, to align LNP production with quality-by-design (QbD) principles, as promoted by regulatory authorities. By leveraging the different stages of the self-assembly process, the method enables greater control over the critical quality attributes. This implies that early stage development can be shortened drastically, thereby accelerating the time-to-market for new LNP therapeutics. From a process engineering perspective, the presented model represents a step toward a predictive process model, streamlining process development even further. The model could be further refined by integrating mechanistic components, such as buffer behavior modeled via Derjaguin−Landau−Verwey−Overbeek theory.[45] For companies, the broad tunable size range enabled by the size/morphology-control method also offers strategic advantages, including potential intellectual property benefits by extending the patent scope and enhancing market exclusivity. The size-control method also enables more fundamental studies: the presented method can be used to probe self-assembly time scales and conditions (SI pp 41 and 42).

Initial in vitro results suggest that LNP efficacy can be enhanced through independent control of the particle size and morphology. Future work should expand on this foundation with systematic in vitro studies across diverse cell types and in vivo evaluation in small animal models and nonhuman primates to assess the translational relevance of morphology- and size-engineered LNPs. The method could, for example, facilitate effective interspecies translation of LNP therapeutics by enabling precise adjustment of the particle size to account for size-dependent differences between rodent models and primates in clinical development.[46]

CONCLUSIONS

LNP formulation is a multistep, kinetically controlled process initiated by mixing two streams. This implies that each step can be selectively influenced and tuned toward specific outcomes. Yet, in practice, these steps are typically collapsed into a single mixing event, limiting tunability and obscuring mechanistic control. This study presents a size- and morphology-control method that shifts LNP production from an empirical mixing-dominant methodology to a rational, design-driven process. By decoupling the multistep LNP formation process into an initial self-assembly stage, followed by a fusion-dominated growth phase with a timed kinetic quench, the method enables independent and predictive control over the particle size and morphology, critical quality attributes that strongly influence LNP efficacy. The approach is robust across formulations, flow rates, and mixer geometries and is supported by a simple, data-driven model for process prediction and control. This implies that the size- and morphology-control method is suitable for manufacturing LNPs. Importantly, LNPs produced using this method maintain high EE, lipid homogeneity, and internal structure and exhibit higher in vitro transfection across multiple conditions. These findings lay a strong foundation for scalable, QbD-aligned LNP manufacturing and open opportunities for translational optimization across cell types and species.

METHODS/EXPERIMENTAL

Impinging Jet Mixing Manufacturing Platform. Unless otherwise specified, a benchtop NanoScaler IJM (Knauer GmbH) equipped with a proprietary impingement jet mixer, featuring a glass observation window and subject to a nondisclosure agreement (NDA), was used. For the size-control method, another geometrically similar IJM, also subject to an NDA, was used. The two mixers are connected via tubing designed to impose a defined residence time (5−1000 ms). LNP samples were analyzed with a spatially resolved dynamic light scattering (SR-DLS) instrument, a NanoFlowSizer (InProcess LSP), operated in batch (vial) mode. The time difference between the formulation and size measurement was around 60 s. Additional information is detailed in the SI.

Benchmark Formulation. Unless stated otherwise, all results presented here were obtained using a "benchmark LNP formulation", in which a standard lipid mixture dissolved in ethanol (200 Proof, molecular biology grade) was mixed with an acidic aqueous (RNase-free) buffer containing the cargo.

The benchmark lipid mixture consisted of [(4-hydroxybutyl)-azanediyl]di(hexane-6,1-diyl)bis(2-hexyldecanoate) (ALC-0315), cholesterol, 1,2-distearoyl-*sn*-glycero-3-phosphocholine (DSPC), and 1,2-dimyristoyl-*rac*-glycero-3-methoxypoly(ethylene glycol)-2000 (DMG-PEG2000) at molar ratios of 50:38.5:10:1.5. Variations in the ionizable lipid type or molar ratios are explicitly noted where applicable. The benchmark aqueous phase consisted of a 100 mM sodium acetate buffer at pH 5.5, containing either purified mRNA [COVID-19 (4278 nucleotides) and FLuc (2112 nucleotides)], yeast RNA (purified Torulla Ambion), poly(A) (700−3500 kDa), or no cargo (drug-free). The cargo is explicitly stated for all presented experiments. In some experiments, the buffer strength, pH, or composition were varied; unless otherwise indicated, sodium acetate was used. In selected cases, a citric acid buffer was substituted.

The lipid−ethanol stock solution was prepared at 10 mg/mL for FRR = 3:1 and 5 mg/mL for FRR = 1:1 and the size-control method, ensuring a consistent final lipid concentration across all conditions. For mRNA cargo, the aqueous buffer concentration was adjusted to maintain a N/P ratio of 6, unless otherwise specified. Yeast RNA and poly(A) were used at the same concentration as that for FLuc mRNA.

Full details on materials and reagents are provided in the SI.

LNP Formulation. Prior to each experiment, the setup was cleaned with Triton X-100 and RNase-Away solutions. Between runs, the system was flushed with RNase-free water, and the tubing was cleared to prevent cross-contamination.

Unless otherwise specified, the total flow rate in the first IJM mixer was maintained at 20 mL/min. For the size-control method, the total flow rate was maintained at 40 mL/min. To account for the dead volume, stationary fluid was initially diverted to waste. The system was operated for at least five residence times before switching to sample collection, ensuring steady-state conditions. A minimum of 2.5 mL was collected per sample by automated valve switching. All pump pressures were continuously monitored during operation with no fouling observed. All reported conditions were measured in triplicate.

Additional details on the LNP formulation protocol are discussed in SI pp 8−10.

LNP Characterization. Characterization of the sample was carried out in multiple stages to characterize different aspects of the LNP particles. Conductivity and dynamic light scattering (DLS) measurements were performed immediately after manufacturing to evaluate the initial physicochemical properties, including the ion content and particle size distribution. Particle size distributions were measured via SR-DLS at room temperature (25 °C) using phase-sensitive detection in vial mode, unless specifically stated otherwise. The refractive index and viscosity settings reflected only solvent contributions. For batch mode, ≥5 replicates (7 s each) were acquired per sample. Large particle detection was enabled when needed. Daily calibration was performed using 30−150 nm polystyrene standards.

https://doi.org/10.1021/acsnano.5c09800
ACS Nano XXXX, XXX, XXX−XXX

Small-angle X-ray scattering (SAXS), SPARTA analyses, and encapsulation efficiencies were conducted after the sample had been stored at 4 °C. Selected samples were dialyzed to neutral pH (1x PBS, pH 7.4) prior to transfection assay and cryo-transmission electron microscopy (cryoTEM) measurements to assess the in vitro performance and visualize the morphology at high resolution, respectively. CryoTEM imaging was performed on a JEOL 2100 field-emission-gun microscope (200 kV) using a low-dose protocol, with magnifications of 10000−60000×. Images were acquired with a Gatan 2kx2k UltraScan CCD camera. Bleb-like particle fractions were quantified manually by counting at least 300 individual particles.

Additional details on the LNP characterization are discussed in SI pp 11−14.

In Vitro Transfection. Lenti-X 293T cells were cultured in Dulbecco's modified Eagle's medium with 10% fetal bovine serum and 1× antibiotic−antimycotic at 37 °C and 5% CO_2 and passaged at 80% confluency using TrypLE. For transfection, 10000 cells/well were seeded in 96-well plates (250 μL/well) 24 h prior. On transfection day, the medium was replaced with 200 μL of a LNP-containing medium (100 ng mRNA/well); each LNP was tested in triplicate across three plates. Controls used Lipofectamine MessengerMAX (0.15 μL/well) with 100 ng of FLuc mRNA. After 24 h, luminescence was assessed using the ONE-Glo EX system (Promega). A total of 100 μL of the medium was replaced with a reagent using an Integra Assist Plus; plates were incubated 3 min in the dark and then read on a Tecan Spark Cyto (3 min shake, 500 ms integration, OD2). Raw counts per second were median-collapsed across technical replicates.

Additional details on the LNP in vitro transfection protocol are discussed in SI p 15.

Other. Additional information regarding the methods is provided in SI pp 1−55.

ASSOCIATED CONTENT

Data Availability Statement

All experimental data are available in the main text or the Supporting Information. All figures were created using BioRender.com, Devos, C. (2025).

Supporting Information

The Supporting Information is available free of charge at https://pubs.acs.org/doi/10.1021/acsnano.5c09800.

Details on the physical and chemical tracer tests for IJM, along with experimental protocols for LNP formulation and characterization, additional results including data regarding mean particle sizes, size distributions, structural and morphological characterization, and model-based LNP size prediction, materials and methods, Figures S1−S42, Tables S1−S6, and references (PDF)

AUTHOR INFORMATION

Corresponding Author

Allan S. Myerson − *Department of Chemical Engineering, Massachusetts Institute of Technology, Cambridge, Massachusetts 02139, United States;* orcid.org/0000-0002-7468-8093; Email: myerson@mit.edu

Authors

Cedric Devos − *Department of Chemical Engineering, Massachusetts Institute of Technology, Cambridge, Massachusetts 02139, United States;* orcid.org/0000-0002-8154-4872

Aniket Udepurkar − *Department of Chemical Engineering, Massachusetts Institute of Technology, Cambridge, Massachusetts 02139, United States;* orcid.org/0000-0001-9958-412X

Peter Sagmeister − *Department of Chemical Engineering, Massachusetts Institute of Technology, Cambridge, Massachusetts 02139, United States;* orcid.org/0000-0002-4326-1775

Ariana S. Hodlewsky − *Department of Chemical Engineering, Massachusetts Institute of Technology, Cambridge, Massachusetts 02139, United States*

Julie Chen − *Department of Chemical Engineering, Massachusetts Institute of Technology, Cambridge, Massachusetts 02139, United States*

Andrew Hatas − *Department of Chemical Engineering, Massachusetts Institute of Technology, Cambridge, Massachusetts 02139, United States*

Nicole Ostrovsky − *Koch Institute for Integrative Cancer Research, Massachusetts Institute of Technology, Cambridge, Massachusetts 02139, United States*

Mushriq Al-Jazrawe − *Koch Institute for Integrative Cancer Research, Massachusetts Institute of Technology, Cambridge, Massachusetts 02139, United States*

Joy I. Ren − *Department of Chemical Engineering, Massachusetts Institute of Technology, Cambridge, Massachusetts 02139, United States*

Andy Y. Liu − *Department of Chemical Engineering, Massachusetts Institute of Technology, Cambridge, Massachusetts 02139, United States*

Richard D. Braatz − *Department of Chemical Engineering, Massachusetts Institute of Technology, Cambridge, Massachusetts 02139, United States;* orcid.org/0000-0003-4304-3484

Complete contact information is available at: https://pubs.acs.org/10.1021/acsnano.5c09800

Author Contributions

†C.D., A.U., and P.S. contributed equally to this work. Conceptualization: C.D., A.U., P.S., and A.S.M. Methodology: C.D., A.U., P.S., and A.S.M. Investigation: C.D., A.U., P.S., A.S.H., J.C., A.H., N.O., M.A.-J., J.I.R., and A.Y.L. Funding acquisition: R.D.B. and A.S.M. Supervision: R.D.B. and A.S.M. Writing—original draft: C.D., A.U., P.S., and A.S.M. Writing—review and editing: C.D., A.U., P.S., A.S.H., J.C., A.H., N.O., M.A.-J., J.I.R., A.Y.L., R.D.B., and A.S.M.

Notes

The authors declare no competing financial interest.

ACKNOWLEDGMENTS

This research was supported by the U.S. Food and Drug Administration under the FDA BAA-22-00123 program (Award 75F40122C00200). This work was also supported in part by the Koch Institute Support (core) Grant P30-CA14051 from the National Cancer Institute. We thank the Koch Institute's Robert A. Swanson (1969) Biotechnology Center for technical support, specifically the Peterson (1957) Nanotechnology Materials Core Facility and the High Throughput Sciences Core Facility (RRID:SCR_026340). The SAXS characterization was performed in the MIT.Nano characterization facilities.

REFERENCES

(1) Udepurkar, A.; Devos, C.; Sagmeister, P.; Destro, F.; Inguva, P.; Ahmadi, S.; Boulais, E.; Quan, Y.; Braatz, R. D.; Myerson, A. S. Structure and Morphology of Lipid Nanoparticles for Nucleic Acid Drug Delivery: A Review. *ACS Nano* **2025**, *19*, 21206−21242.

(2) Cullis, P. R.; Felgner, P. L. The 60-year evolution of lipid nanoparticles for nucleic acid delivery. *Nat. Rev. Drug Discovery* **2024**, *23*, 709−722.
(3) Hamilton, A. G.; Swingle, K. L.; Mitchell, M. J. Biotechnology: Overcoming biological barriers to nucleic acid delivery using lipid nanoparticles. *PLOS Biology* **2023**, *21*, e3002105.
(4) Hou, X.; Zaks, T.; Langer, R.; Dong, Y. Lipid nanoparticles for mRNA delivery. *Nature Reviews Materials* **2021**, *6*, 1078−1094.
(5) Kon, E.; Ad-El, N.; Hazan-Halevy, I.; Stotsky-Oterin, L.; Peer, D. Targeting cancer with mRNA-lipid nanoparticles: key considerations and future prospects. *Nature Reviews Clinical Oncology* **2023**, *20*, 739−754.
(6) Chaudhary, N.; Weissman, D.; Whitehead, K. A. mRNA vaccines for infectious diseases: principles, delivery and clinical translation. *Nat. Rev. Drug Discovery* **2021**, *20*, 817−838.
(7) Mitchell, M. J.; Billingsley, M. M.; Haley, R. M.; Wechsler, M. E.; Peppas, N. A.; Langer, R. Engineering precision nanoparticles for drug delivery. *Nat. Rev. Drug Discovery* **2021**, *20*, 101−124.
(8) Swingle, K. L.; Safford, H. C.; Geisler, H. C.; Hamilton, A. G.; Thatte, A. S.; Billingsley, M. M.; Joseph, R. A.; Mrksich, K.; Padilla, M. S.; Ghalsasi, A. A.; Alameh, M.-G.; Weissman, D.; Mitchell, M. J. Ionizable Lipid Nanoparticles for In Vivo mRNA Delivery to the Placenta during Pregnancy. *J. Am. Chem. Soc.* **2023**, *145*, 4691−4706.
(9) Miao, L.; Li, L.; Huang, Y.; Delcassian, D.; Chahal, J.; Han, J.; Shi, Y.; Sadtler, K.; Gao, W.; Lin, J.; Doloff, J. C.; Langer, R.; Anderson, D. G. Delivery of mRNA vaccines with heterocyclic lipids increases anti-tumor efficacy by STING-mediated immune cell activation. *Nat. Biotechnol.* **2019**, *37*, 1174−1185.
(10) Xue, L.; Gong, N.; Shepherd, S. J.; Xiong, X.; Liao, X.; Han, X.; Zhao, G.; Song, C.; Huang, X.; Zhang, H.; Padilla, M. S.; Qin, J.; Shi, Y.; Alameh, M.-G.; Pochan, D. J.; Wang, K.; Long, F.; Weissman, D.; Mitchell, M. J. Rational Design of Bisphosphonate Lipid-like Materials for mRNA Delivery to the Bone Microenvironment. *J. Am. Chem. Soc.* **2022**, *144*, 9926−9937.
(11) Xue, L.; Zhao, G.; Gong, N.; Han, X.; Shepherd, S. J.; Xiong, X.; Xiao, Z.; Palanki, R.; Xu, J.; Swingle, K. L.; Warzecha, C. C.; El-Mayta, R.; Chowdhary, V.; Yoon, I.-C.; Xu, J.; Cui, J.; Shi, Y.; Alameh, M.-G.; Wang, K.; Wang, L.; Pochan, D. J.; Weissman, D.; Vaughan, A. E.; Wilson, J. M.; Mitchell, M. J. Combinatorial design of siloxane-incorporated lipid nanoparticles augments intracellular processing for tissue-specific mRNA therapeutic delivery. *Nat. Nanotechnol.* **2025**, *20*, 132.
(12) Witten, J.; Raji, I.; Manan, R. S.; Beyer, E.; Bartlett, S.; Tang, Y.; Ebadi, M.; Lei, J.; Nguyen, D.; Oladimeji, F.; Jiang, A. Y.; MacDonald, E.; Hu, Y.; Mughal, H.; Self, A.; Collins, E.; Yan, Z.; Engelhardt, J. F.; Langer, R.; Anderson, D. G. Artificial intelligence-guided design of lipid nanoparticles for pulmonary gene therapy. *Nat. Biotechnol.* (**2024**). DOI: 10.1038/s41587-024-02490-y
(13) Shepherd, S. J.; Han, X.; Mukalel, A. J.; El-Mayta, R.; Thatte, A. S.; Wu, J.; Padilla, M. S.; Alameh, M.-G.; Srikumar, N.; Lee, D.; Weissman, D.; Issadore, D.; Mitchell, M. J. Throughput-scalable manufacturing of SARS-CoV-2 mRNA lipid nanoparticle vaccines. *Proc. Natl. Acad. Sci. U.S.A.* **2023**, *120*, e2303567120.
(14) Cui, L.; Hunter, M. R.; Sonzini, S.; Pereira, S.; Romanelli, S. M.; Liu, K.; Li, W.; Liang, L.; Yang, B.; Mahmoudi, N.; Desai, A. S. Mechanistic Studies of an Automated Lipid Nanoparticle Reveal Critical Pharmaceutical Properties Associated with Enhanced mRNA Functional Delivery In Vitro and In Vivo. *Small* **2022**, *18*. DOI: 10.1002/smll.202105832
(15) Zhang, T.; Yin, H.; Li, Y.; Yang, H.; Ge, K.; Zhang, J.; Yuan, Q.; Dai, X.; Naeem, A.; Weng, Y.; Huang, Y.; Liang, X.-J. Optimized lipid nanoparticles (LNPs) for organ-selective nucleic acids delivery in vivo. *Publisher* **2024**, *27*, 109804.
(16) Liao, S.; Wang, S.; Wadhwa, A.; Birkenshaw, A.; Fox, K.; Cheng, M. H. Y.; Casmil, I. C.; Magana, A. A.; Bathula, N. V.; Ho, C. H.; Cheng, J.-Y.; Foster, L. J.; Harder, K. W.; Ross, C. J. D.; Cullis, P. R.; Blakney, A. K. Transfection Potency of Lipid Nanoparticles Containing mRNA Depends on Relative Loading Levels. *ACS Appl. Mater. Interfaces* **2025**, *17*, 3097−3105.
(17) Cheng, M. H. Y.; Leung, J.; Zhang, Y.; Strong, C.; Basha, G.; Momeni, A.; Chen, Y.; Jan, E.; Abdolahzadeh, A.; Wang, X.; Kulkarni, J. A.; Witzigmann, D.; Cullis, P. R. Induction of Bleb Structures in Lipid Nanoparticle Formulations of mRNA Leads to Improved Transfection Potency. *Adv. Mater.* **2023**, *35*, 2303370.
(18) Cheng, M. H. Y.; Zhang, Y.; Fox, K.; Leung, J.; Strong, C.; Kang, E.; Chen, Y.; Tong, M.; Bommadevara, H.; Jan, E.; Ip, O. Y. L.; Rodríguez-Rodríguez, C.; Saatchi, K.; Häfeli, U. O.; Abdolahzadeh, A.; Witzigmann, D.; Cullis, P. R. Liposomal lipid nanoparticles for extrahepatic delivery of mRNA. *Nat. Commun.* **2025**, *16*, 4135.
(19) Hassett, K. J.; Higgins, J.; Woods, A.; Levy, B.; Xia, Y.; Hsiao, C. J.; Acosta, E.; Almarsson, Ö.; Moore, M. J.; Brito, L. A. Impact of lipid nanoparticle size on mRNA vaccine immunogenicity. *J. Controlled Release* **2021**, *335*, 237−246.
(20) He, Z.; Hu, Y.; Nie, T.; Tang, H.; Zhu, J.; Chen, K.; Liu, L.; Leong, K. W.; Chen, Y.; Mao, H.-Q. Size-controlled lipid nanoparticle production using turbulent mixing to enhance oral DNA delivery. *Acta Biomaterialia* **2018**, *81*, 195−207.
(21) Chen, D.; Liu, Z.; Guo, L.; Yang, L.; Zhao, Y.; Yang, M. Controlled preparation of lipid nanoparticles in microreactors: Mixing time, morphology and mRNA delivery. *Chemical Engineering Journal* **2025**, *505*, 159318.
(22) Ripoll, M.; Martin, E.; Enot, M.; Robbe, O.; Rapisarda, C.; Nicolai, M.-C.; Deliot, A.; Tabeling, P.; Authelin, J.-R.; Nakach, M.; Wils, P. Optimal self-assembly of lipid nanoparticles (LNP) in a ring micromixer. *Sci. Rep.* **2022**, *12*, 9483.
(23) Pial, T. H.; Li, S.; Lin, J.; Wang, T.-H.; Mao, H.-Q.; Curk, T. Controlling Payload Heterogeneity in Lipid Nanoparticles for RNA-Based Therapeutics. *bioRxiv*, version 1; 2025. DOI: 10.1101/2025.06.11.659145 (accessed August 15, 2025).
(24) Okuda, K.; Sato, Y.; Iwakawa, K.; Sasaki, K.; Okabe, N.; Maeki, M.; Tokeshi, M.; Harashima, H. On the size-regulation of RNA-loaded lipid nanoparticles synthesized by microfluidic device. *J. Controlled Release* **2022**, *348*, 648−659.
(25) Binici, B.; Borah, A.; Watts, J. A.; McLoughlin, D.; Perrie, Y. The influence of citrate buffer molarity on mRNA-LNPs: Exploring factors beyond general critical quality attributes. *Int. J. Pharm.* **2025**, *668*, 124942.
(26) Chander, N.; Basha, G.; Yan Cheng, M. H.; Witzigmann, D.; Cullis, P. R. Lipid nanoparticle mRNA systems containing high levels of sphingomyelin engender higher protein expression in hepatic and extra-hepatic tissues. *Molecular Therapy - Methods & Clinical Development* **2023**, *30*, 235−245.
(27) Kulkarni, J.; Chander, N.; Basha, G.; Ciufolini, M. A.; Witzigmann, D.; Cullis, P. U.S. Patent US0240374754 A1, 2024.
(28) McMillan, C.; Druschitz, A.; Rumbelow, S.; Borah, A.; Binici, B.; Rattray, Z.; Perrie, Y. Tailoring lipid nanoparticle dimensions through manufacturing processes. *RSC Pharmaceutics* **2024**, *1*, 841−853.
(29) Devos, C.; Mukherjee, S.; Inguva, P.; Singh, S.; Wei, Y.; Mondal, S.; Yu, H.; Barbastathis, G.; Stelzer, T.; Braatz, R. D.; Myerson, A. S. Impinging jet mixers: A review of their mixing characteristics, performance considerations, and applications. *AIChE J.* **2025**, *71*, e18595.
(30) Roces, C. B.; Lou, G.; Jain, N.; Abraham, S.; Thomas, A.; Halbert, G. W.; Perrie, Y. Manufacturing Considerations for the Development of Lipid Nanoparticles Using Microfluidics. *Pharmaceutics* **2020**, *12*, 1095.
(31) Patra, M.; Salonen, E.; Terama, E.; Vattulainen, I.; Faller, R.; Lee, B. W.; Holopainen, J.; Karttunen, M. Under the Influence of Alcohol: The Effect of Ethanol and Methanol on Lipid Bilayers. *Biophys. J.* **2006**, *90*, 1121−1135.
(32) Shobhna; Kashyap, H. K. Deciphering Ethanol-Driven Swelling, Rupturing, Aggregation, and Fusion of Lipid Vesicles Using Coarse-Grained Molecular Dynamics Simulations. *Langmuir* **2022**, *38*, 2445−2459.
(33) Kimura, N.; Maeki, M.; Sato, Y.; Ishida, A.; Tani, H.; Harashima, H.; Tokeshi, M. Development of a Microfluidic-Based Post-Treatment Process for Size-Controlled Lipid Nanoparticles and

Application to siRNA Delivery. *ACS Appl. Mater. Interfaces* **2020**, *12*, 34011−34020.
(34) Zhigaltsev, I. V.; Cullis, P. R. Morphological Behavior of Liposomes and Lipid Nanoparticles. *Langmuir* **2023**, *39*, 3185−3193.
(35) Gindy, M. E.; DiFelice, K.; Kumar, V.; Prud'homme, R. K.; Celano, R.; Haas, R. M.; Smith, J. S.; Boardman, D. Mechanism of Macromolecular Structure Evolution in Self-Assembled Lipid Nanoparticles for siRNA Delivery. *Langmuir* **2014**, *30*, 4613−4622.
(36) Kamanzi, A.; Zhang, Y.; Gu, Y.; Liu, F.; Berti, R.; Wang, B.; Saadati, F.; Ciufolini, M. A.; Kulkarni, J.; Cullis, P.; Leslie, S. Quantitative Visualization of Lipid Nanoparticle Fusion as a Function of Formulation and Process Parameters. *ACS Nano* **2024**, *18*, 18191−18201.
(37) Leung, A. K. K.; Hafez, I. M.; Baoukina, S.; Belliveau, N. M.; Zhigaltsev, I. V.; Afshinmanesh, E.; Tieleman, D. P.; Hansen, C. L.; Hope, M. J.; Cullis, P. R. Lipid Nanoparticles Containing siRNA Synthesized by Microfluidic Mixing Exhibit an Electron-Dense Nanostructured Core. *J. Phys. Chem. C* **2012**, *116*, 18440−18450.
(38) Kulkarni, J. A.; Witzigmann, D.; Leung, J.; Van Der Meel, R.; Zaifman, J.; Darjuan, M. M.; Grisch-Chan, H. M.; Thöny, B.; Tam, Y. Y. C.; Cullis, P. R. Fusion-dependent formation of lipid nanoparticles containing macromolecular payloads. *Nanoscale* **2019**, *11*, 9023−9031.
(39) Schariter, J.; Hassett, K.; Smith, M.; Almarsson, O.; Brito, L. U.S. Patent US11,744,801 B2, 2020.
(40) Wang, H.; Pestre, H.; Tan, E.-K. N.; Wedemann, L.; Schuhmacher, J. S.; Schuhmacher, M.; Stellacci, F. Facile lipid nanoparticle size engineering approach via controllable fusion induced by depletion forces. *J. Colloid Interface Sci.* **2025**, *691*, 137334.
(41) Rennick, J. J.; Johnston, A. P. R.; Parton, R. G. Key principles and methods for studying the endocytosis of biological and nanoparticle therapeutics. *Nat. Nanotechnol.* **2021**, *16*, 266−276.
(42) Kranz, L. M.; Diken, M.; Haas, H.; Kreiter, S.; Loquai, C.; Reuter, K. C.; Meng, M.; Fritz, D.; Vascotto, F.; Hefesha, H.; Grunwitz, C.; Vormehr, M.; Hüsemann, Y.; Selmi, A.; Kuhn, A. N.; Buck, J.; Derhovanessian, E.; Rae, R.; Attig, S.; Diekmann, J.; Jabulowsky, R. A.; Heesch, S.; Hassel, J.; Langguth, P.; Grabbe, S.; Huber, C.; Türeci, Ö.; Sahin, U. Systemic RNA delivery to dendritic cells exploits antiviral defence for cancer immunotherapy. *Nature* **2016**, *534*, 396−401.
(43) Hu, Y.; Tzeng, S. Y.; Cheng, L.; Lin, J.; Villabona-Rueda, A.; Yu, S.; Li, S.; Schneiderman, Z.; Zhu, Y.; Ma, J.; Wilson, D. R.; Shannon, S. R.; Warren, T.; Rui, Y.; Qiu, C.; Kavanagh, E. W.; Luly, K. M.; Zhang, Y.; Korinetz, N.; D'Alessio, F. R.; Wang, T.-H.; Kokkoli, E.; Reddy, S. K.; Luijten, E.; Green, J. J.; Mao, H.-Q. Supramolecular assembly of polycation/mRNA nanoparticles and in vivo monocyte programming. *Proc. Natl. Acad. Sci. U.S.A.* **2024**, *121*, 121.
(44) Inguva, P. K.; Mukherjee, S.; Walker, P. J.; Tenberg, V.; Devos, C.; Shin, S.; Wu, Y.; Santra, S.; Wang, J.; Singh, S.; Kanso, M. A.; Kim, S. H.; Trout, B. L.; Bazant, M. Z.; Myerson, A. S.; Braatz, R. D. Mechanistic modeling of lipid nanoparticle formation for the delivery of nucleic acid therapeutics. *Biotechnology Advances* **2025**, *84*, 108643.
(45) Shin, S.; Devos, C.; Udepurkar, A. P.; Inguva, P. K.; Myerson, A. S.; Braatz, R. D. Mechanistic modeling of lipid nanoparticle (LNP) precipitation via population balance equations (PBEs). *Chemical Engineering Journal* **2025**, 167786.
(46) Lam, K.; Schreiner, P.; Leung, A.; Stainton, P.; Reid, S.; Yaworski, E.; Lutwyche, P.; Heyes, J. Optimizing Lipid Nanoparticles for Delivery in Primates. *Adv. Mater.* **2023**, *35*, 2211420.

https://doi.org/10.1021/acsnano.5c09800
ACS Nano XXXX, XXX, XXX−XXX